Semnan University

Progress in Physics of Applied Materials

journal homepage: https://ppam.semnan.ac.ir/

Fabrication of multi-layer antireflection coating consisting of ZnS and MgF_2

R. Zarei Moghadam[a*], H. Omrani[a], M. Taherkhani[a], F. Shokrian[b]

[a] *Faculty of Physics, Semnan University, Semnan, Iran*
[b] *Education of Semnan province, Semnan, Iran*

ARTICLE INFO

Article history:
Received: 7 May 2021
Revised: 5 June 2021
Accepted: 12 June 2021

Keywords:
Antireflection coating
GLAD technique
XRD analysis
Refractive index

ABSTRACT

In this study, Magnesium Fluoride (MgF_2) and Zinc Sulfide (ZnS) multi-layer antireflection coatings were prepared using Glancing Angle Deposition (GLAD) technique. MgF_2 and ZnS materials have been coated in a Hind - Hivac coating unit (model 15F) on glass substrates. Antireflection coatings were prepared at different oblique incident flux angles (α = 40°, 65°,70°, 80°) by the thermal evaporation method. The Grazing incidence X-ray diffraction (GIXRD)analysis indicated that the thin films coated at different incident angles were crystallized in a single phase with an orthorhombic structure. The XRD results showed improvement of the film crystallinity upon grain size increment. Optical properties were investigated throughout the measurement of transmission spectra and refractive index and extinction in the visible region. The refractive index of films decreased from 2.8 to 1.66 as the flux angle increases from 40° to 80°. The extinction coefficient of films increased from 0.03849 to 0.05997 as the flux angle increases from 40° to 80°.

1. Introduction

Anti-Reflection coatings (ARc) utilize interference to control the reflection parameter. The interference at a medium boundary occurs due to the change of the refractive index. The vast usages of thin films are essential in various systems [1]. One of their essential important applications is in solar cells [2-4]. Reflectance loss is the original, challenging phenomenon in solar cells or any other optical system. When sunlight crossing crosses from them, efficiency is reduced [2,3,5]. Currently, the surface treatment techniques used to provide solar cells to assemble light effectively contain surface texturing and antireflection coating formation [6,7]. Handling an antireflection coating on a solar cell decreases the reflectance to less than three layers [8]. Newly, silicon nitride coatings, which include hydrogen acting as surface passivation, and antireflection coatings have been used [8]. MgF_2 has achieved high consideration in research and has become a standard material for optical systems. MgF_2 is a material with a low absorption coefficient, high refractive index, excellent transparency, and good chemical stabilities [9, 10]. The excellent transparency of MgF_2 has led to its use in optical systems. MgF_2, when used as a coating on optical windows lenses, is an excellent ideal antireflection property. ZnS is a significant broad bandgap semiconductor which extensively used in optical systems. It has a reflection loss of 24.7% and a refractive index of 2.2 [11]. ZnS is a practical suitable material for use in antireflection films [3-5,12] due to its particular properties such as high versatility, broad bandgap, high transmission, and low cost [12-15]. One of the suitable methods to manufacture of the ZnS films is physical vapor deposition (PVD) technique. Because it has unique advantages such as; low cost of operation, low material consumption, high deposition rate [16], capability in controlling the substrate condition [17]. The thin films of MgF_2 and ZnS are easily prepared with high optical quality using thermal evaporation systems, which makes making the materials suitable for applications in optical devices [18–20]. The most outstanding feature of ZnS is that ZnS is high refractive index material like TiO2, but experiences a lower chemical decomposition process during non-reactive deposition compared to that of TiO_2. Also, MgF_2 is low refractive index material like SiO_2, but it is easily prepared by non-reactive deposition at lower deposition temperature with a higher deposition rate. For GLAD, the deposition rate is a very important factor because slanting deposition nature of the GLAD technique severely reduces deposition rate. To achieve multilayer growth, an in-depth investigation into the growth properties was performed. Therefore, ZnS with a high refractive index and MgF_2 with a low refractive index are commonly used for single, double-layer, and triple-layer AR

* Corresponding author. Tel.: +989140104665
E-mail address: r.zarei1991@gmail.com

DOI: 10.22075/PPAM.2021.23357.1005

coatings. Generally, refractive indices of ZnS and MgF2 are known to be 2.354 and 1.377 at 630 nm, respectively [21]. At present, many potential applications of ZnS and MgF_2, such as LEDs, solar cells, photo-detectors, photovoltaic cells, solar collectors, IR diodes [21], etc. are being explored. The thin films of ZnS and MgF_2 have been prepared by many deposition techniques such as thermal evaporation [22], sputtering [23], chemical bath deposition [24], SILAR [25], thermionic vacuum arc (TVA) [26], spray pyrolysis [27], and others [28, 29].

The GLAD method has been developed since the researchers found that they could manipulate column structures with the active management of substrate location within the address layer. Although GLAD has significant advances over the last 20 years, its complex research is still not well understood, and the results of empirical studies are not very consistent with theoretical studies. One of the most essential factors in this method is the layer that has a significant effect on the formation of motility. The impact of the shadow of this phenomenon occurs more on the level of the impaction layer. Some researchers have performed MgF_2 coatings using the GLAD technique. Chun Guo et al. [30] deposited the MgF_2 coatings at different oblique incident flux angles and studied the effect of increasing the flux angle on structural and optical properties.

In this paper, MgF_2 and ZnS multi-layer ARc (single-layer, double, and triple layer) was studied. ZnS and MgF_2 films were deposited by the PVD method. The optical properties of films were systematically investigated as a function of deposition angles. In addition, simulated results of ARc were compared to experimental results. The film thickness and film angles were found out using images obtained by FESEM, and with the help of the Digimizer software. The structural properties of films were studied using XRD patterns.

2. Experimental

MgF_2 and ZnS materials have been coated in a Hind - Hivac coating unit (model 15F6) on glass substrates. The deposition was carried out using the PVD method by using thermally heated source in a vacuum chamber. For manufacturing oblique films, the substrates were oriented 80° to the source around normal axis, with the help of the system shown in Fig. 1. Also, to fabricate a normal common and inclined combination layer, the process was performed in a single run without opening the chamber. The pressure of the chamber was 1×10^{-5} mbar and working at room temperature. Before deposition processes, the substrates in an ultrasonic bath were washed with soap and water solution and then washed with acetone, and dried by nitrogen gas. MgF_2 (purity: 99.99%) and ZnS (99.99%) compounds supplied by Sigma Aldrich Company, were placed in molybdenum source. The deposition thickness and deposition rate of the coatings were controlled by a piezoelectric crystal. The deposition rates were 4 Å/s. The distance between the evaporation source and the substrate was 23cm. The distance between the piezoelectric crystal and evaporation source was 25cm. During the process using a circulating water system, the substrate temperature was kept at 70 °C. Five samples were prepared with different growth conditions and given in Table 1. As exhibited, two types of ZnS and MgF_2 films, including single and multi-layer coatings, were fabricated. For fabricating the inclined combination layer, the process was performed in a single run without opening the chamber. Optical properties were studied using a UV–Vis spectrophotometer (PerkinElmer model Lambda-25) in the wavelength range of 300-1200 nm. Morphological properties were analyzed using FESEM (Zeiss model). Structural properties were analyzed using XRD (ADVANCE–D8 model, λ=1.5406Å).

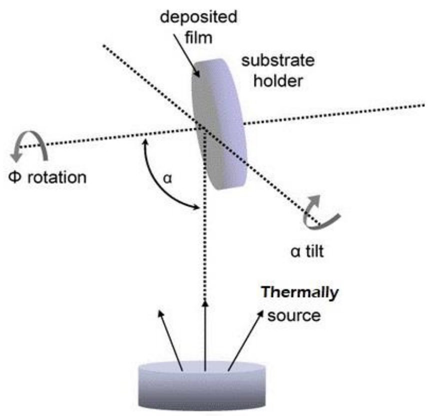

Fig. 1. The schematic diagram of substrate translocation.

Table 1
specifications introducing the prepared coatings.

Sample	**S1**	**S2**	**S3**	**S4**
Number of the deposition layers	1	2	2	2
Deposition angle (degree)	70	40	65	80
film	MgF_2	MgF_2/ZnS	MgF_2/ZnS	MgF_2/ZnS

3. Results and discussion

3.1 FESEM analysis

The FESEM analysis was used to determine the morphology and the thickness of the layers. Fig. 2 represents the cross-section images of the S_1, S_2, S_3, S_4, and

S_5 samples. Fig. 2 shows porous and obliquely column structure. The relation between columnar angle (β) and the incident vapor flow angle (α) is given by the following formula [31-33]:

$$\text{For } \alpha < 60 \quad \tan\beta = 1/2\,(\tan\alpha) \tag{1}$$

$$\text{and for } \alpha > 60 \quad \beta = \alpha - \mathrm{Arc}\sin\,(1 - \cos\alpha)/2 \tag{2}$$

The thickness and angles of the layers, and the growth columnar angle were obtained using Digimizer software. The thicknesses obtained are equal to: S_1 (198 nm), S_2 (216 nm/294.8 nm), S_3 (294 nm/214 nm), S_4 (266 nm/223 nm), and S_5 (244 nm/202 nm/143 nm). The angles obtained are equal to: S_1 (74.58°), S_2 (24.60°/ 38.48°), S_3 (0°/63.74°), S_4 (17.28°/74.31°), and S_5 (0°/19.42°/76.83°). The value of growth columnar angle (β)is calculated for all samples and is presented in Table 2. A good agreement is found between the predicted experimental and theoretical results.

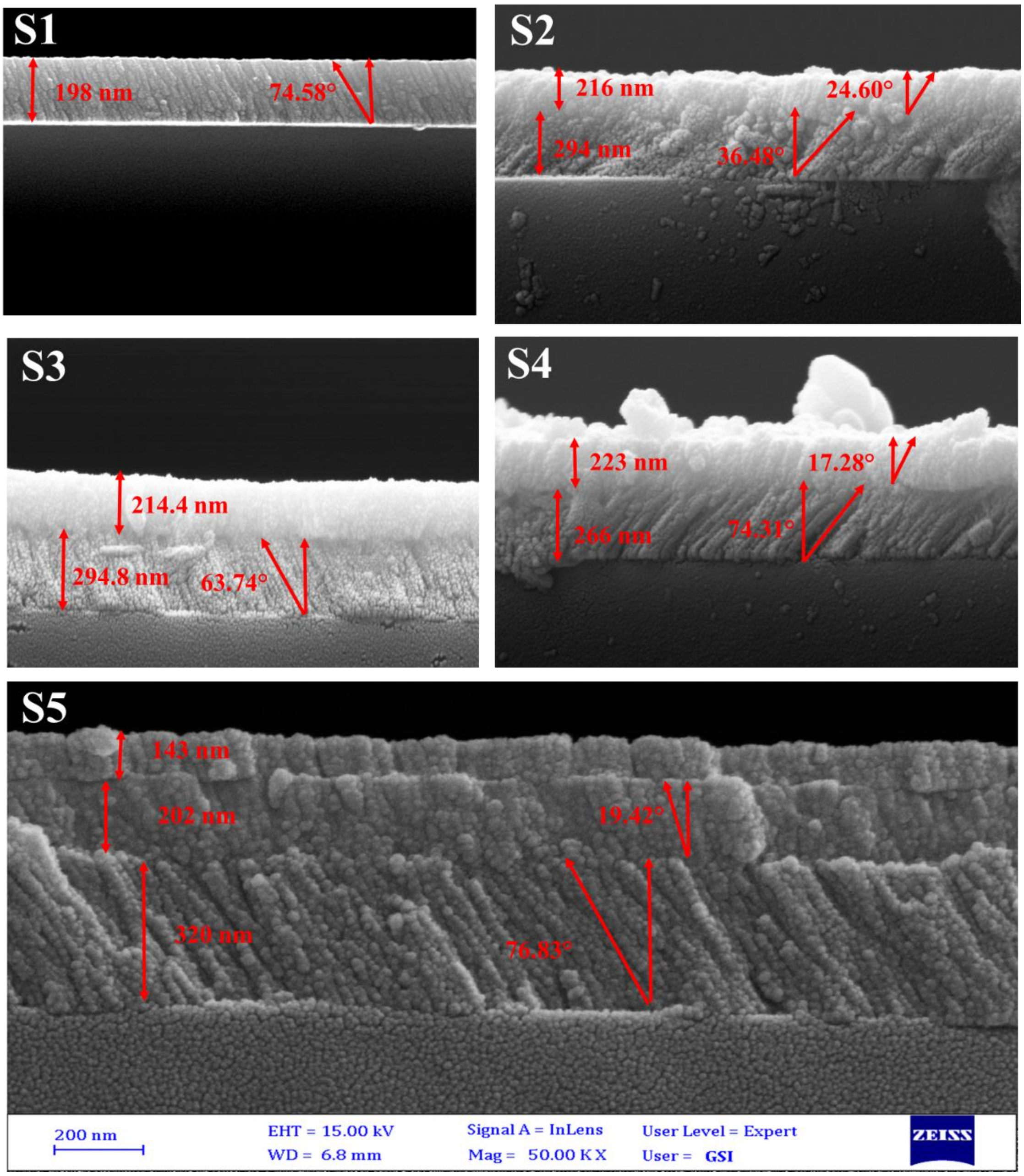

Fig. 2. Cross-sectional FESEM image of MgF_2 / ZnS thin films.

3.2. Structural properties

The structural properties and phase purity of the samples were determined by the GIXRD pattern, as shown in Fig. 3. This figure shows the GIXRD patterns of the S_1, S_2, S_3, S_4, and S_5 samples. The diffractometer system is XPERT-PRO. Using Fig. 3, one can observe tetragonal MgF_2 phase with estimated lattice constants a=3.911±0.002 Å, b=4.516±0.009 Å, c=3.014±0.028 Å, comparable to standard lattice parameters a=4.728 Å, b=4.612 Å, c=3.098

Å (JCPDS:721150) [34]. No impurity phase was observed in the patterns. Using Figure 3, one can observe the cubic phase of ZnS with estimated lattice constants $a = b = c$ = 4.985 ± 0.012 Å as compared to the standard lattice

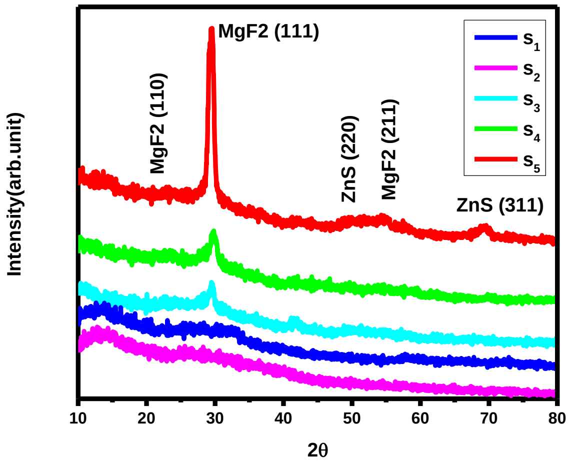

Fig. 3. GIXRD pattern of the S_1, S_2, S_3, S_4, and S_5 samples.

parameters $a = b = c$ = 5.418 Å (JCPDS: 800020) of ZnS [35, 36]. No additional or secondary phase peaks were observed in the XRD pattern of ZnS/MgF2 coating except pristine ZnS and MgF2 peaks, which confirms that during the fabrication of alternate layers in the composite system, the lattice diffusion does not occur. Comparing these data with those of single layers, no additional peaks are found. Then it can be understood that no other crystalline compound is formed during the growth.

The size of the crystal of the samples was obtained with the Debye-Sherrer formula.

$$D = \frac{k\lambda}{\beta\ cos\theta} \qquad (3)$$

Where k is constant (0.9), β is full width at half maximum in radians, λ is *the* source of Cu Kα radiation wavelength (1.54 Å), and D is the size of nanoparticles in nm [37]. Table 2 displays clearly that with the increasing flux angle (from 40 to 80), the crystallinity of the grown films decreases (from S_2 to S_4) which is characteristics of the GLAD technique. But as the number of layers and the thickness of the layers increase, the crystallinity increases (S_5). Improvement of the intensity of peaks indicates the crystallite size increment of the samples, which can be attributed to the shadowing effect [38]. Any extra peaks, as well as secondary phases, were not observed in the combined phases of the ZnS/MgF_2 multilayer except for prior ZnS and MgF_2 peaks, which confirm that the lattice diffusion does not happen during the manufacturing of alternate films in the multilayer system. Single layer and two layers of MgF_2 and ZnS exhibit only little crystallinity, whereas the crystallinity improved with an increase of ZnS/MgF_2 composite.

3.3. Optical properties

One of the most exciting and accessible methods for analyzing nanoparticles is the use of electromagnetic waves in the ultraviolet region, with the optical characteristics of the samples being obtained from the transmittance measurement. Fig. 4 represents the optical transmittance of samples versus wavelength. It is found from Fig. 4 that all of the MgF_2 and ZnS/MgF_2 layers were highly transparent in the broad wavelength region. It can

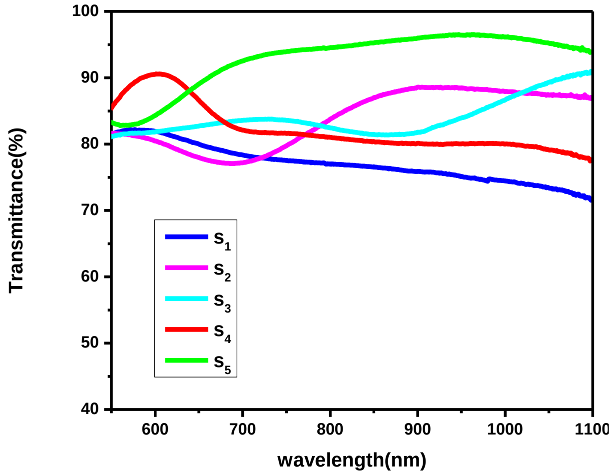

Fig. 4. The transmittance spectra of samples.

be seen that the transmission of the specimens is a function of the angle of the deposition, so that the films with various materials prepared at higher deposition angles demonstrate higher transmission. This may be ascribed to the enhancement in separation distance between the columns, leading to reduced layer density upon applying higher α values [39, 40].

The absorption coefficient (α) for the prepared films was estimated using the following equation [41]:

$$\alpha(\lambda) = -\frac{1}{d}\mathrm{Ln}(T) \qquad (4)$$

Where d is the thickness of films, and T is the transmission of the specimen. Absorption coefficient versus wavelength of samples is shown in Fig. 5. Figure. 5 shows that with increasing the incident flow angle, the absorption coefficient increases. This may be ascribed to the reality that by increasing this flow angle, the porosity of film increases which in turn leads to an increase in roughness of the surface and therefore, an increase in the absorption coefficient. A film with a small absorption coefficient has a flat surface [42]. The higher absorption coefficient of sample S_5 compared with the other four samples may be ascribed to the increase in light trapping in this sample due to its higher porosity. This is well known that the porosity in a structure can cause photon scattering leading to a high absorption coefficient [8, 42].

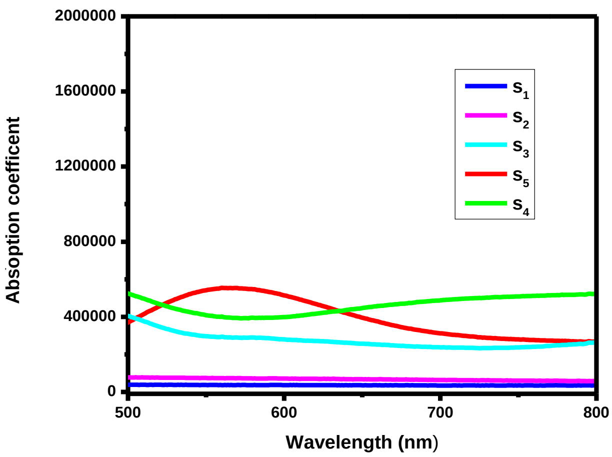

Fig. 5. The absorption coefficient spectra of samples.

The refractive index (n) of the deposited samples was calculated using the following equation [42].

$$n = [H + (H^2 - s^2)^{0.5}]^{0.5} \quad (5)$$

$$H = \frac{4s^2}{(s^2+1)T^2} - \frac{s^2+1}{2} \quad (6)$$

Where H is the Swanepoel constant, T is the transmission , and S is the refractive index of the substrate. Fig. 6 shows, refractive index variations versus the wavelength for MgF_2/ZnS samples. It can be seen from the plots that the refractive index was decreased with absorption coefficient value increment. Similar works also reported the same behavior for the samples produced by the GLAD method [8, 42]. This can be ascribed to the formation of porous structures in the films produced by the GLAD method. In fact, with average surface porosity increment because of using higher incident flow angles, the hollow areas present on the surface facilitated the light passage, which resulted in a refractive index reduction. These results showed that the optical properties of the MgF_2/ZnS layers, such as refractive index, were strongly dependent on the deposition angle. This parameter can pave the way for controlling the optical properties of MgF_2/ZnS films matching our demands. The mean refractive index of the MgF_2/ZnS layers decreases as the deposition angle increases; meanwhile, the extinction coefficient of the samples increases [39].

Table 2
Parameters of MgF2 / ZnS films obtained for samples from optical and microstructure characterization

sample	S_1	S_2	S_3	S_4	S_5
Films	MgF_2	MgF_2/ZnS	MgF_2/ZnS	MgF_2/ZnS	$MgF_2/ZnS/MgF_2$
Thickness (nm)	198	294/216	294.8/214.4	266/223	244/202/143
Angle (°)	74.58	24.60-38.48	0-63.74	17.28-74.31	0-19.42-76.83
β (°)	0.42	0.48	0.52	0.57	0.61
D (nm)	3.4	3.01	2.77	2.52	2.38
T_{max}	83.24	92.80	93.28	92.83	96.7
α (10^5 cm^{-1})	2.36	2.58	2.79	3.56	5.08
n	2.8	2.13	2.05	1.73	1.66
k ($\times 10^{-4}$)	0.029	0.038	0.039	0.045	0.059

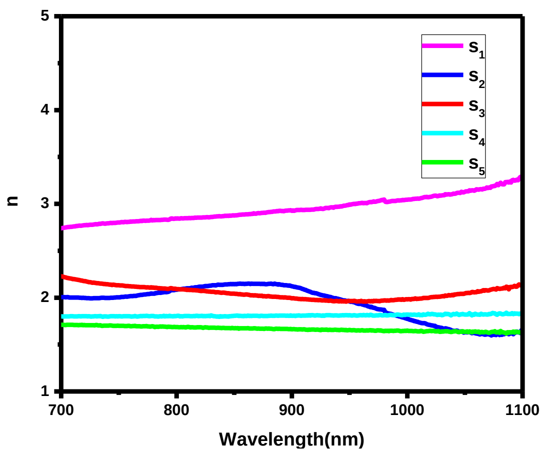

Fig. 6. The refractive index versus wavelength of all the samples.

The extinction coefficient provides information about the light absorption in the medium material due to inelastic scattering. The extinction coefficient is given by $K = \alpha\lambda/(4\pi)$. Here α is the absorption coefficient of the material [40].

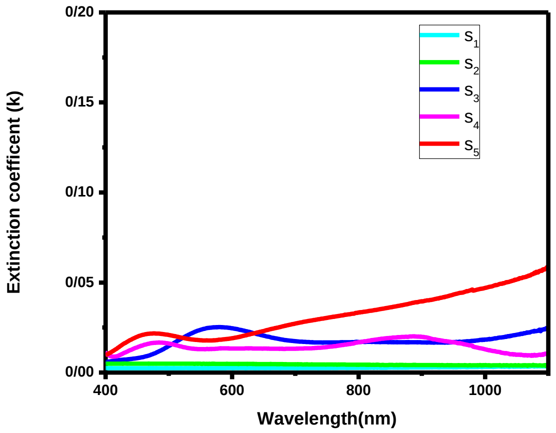

Fig. 7. The extinction coefficient vs. wavelength of all the samples.

Figure 7 shows the extinction coefficient versus wavelength. The extinction coefficient of samples increased from 0.0042 to 0.0016 as the deposition angle increases from 40° to 80°. The low values of k in the visible region are a qualitative indication of the excellent surface smoothness of thin films. Furthermore, the high k-value obtained for α = 80° suggests the presence of significant inhomogeneity in the films (defects, disordering, oxygen vacancies, surface corrugation), especially a rougher film/air interface favored for high glancing angles of deposition [41, 42]. The obtained extinction coefficient results of all the samples are provided in Table. 2.

4. Conclusion

We have studied the design, fabrication, and characterization of the multilayer antireflection coating consisting of ZnS and MgF_2 on the glass substrate. The thin films of MgF2 and ZnS deposited on the glass substrate by GLAD method. The average transmittance of the double-side coated sample increases by about 26% and, its maximum reaches nearly 94%. Using structural analysis of XRD and FESEM, structural properties were studied. The XRD spectra of the samples indicate a reduction in the density and strain of crystalline samples in samples (S_3 and S_4) compared to the S_1 and S_2. These results are consistent with variation in the sample transmittance spectra. The FESEM figures indicate that all the samples were uniform, compact with good adhesion on the ZnS substrate. Also, optical properties are analyzed using UV-Vis analysis. It has been found that with an increase in the deposition angle, the refractive index of the samples is reduced from 2.8 to 1.66. Interesting results were observed with the precipitation of MgF_2 samples at different angles. By increasing the deposition angle, optical transmission ranges (from 550 to 1100 nm) were increased to 96.7 percent. These results introduced these samples as promising candidates for antireflection coatings.

References

[1] R. Zarei Moghadam, H. Ahmadvand, M. Jannesari, Design and fabrication of multi-layers infrared antireflection coating consisting of ZnS and Ge on ZnS substrate, Infrared Phys. Technol. 75 (2016) 18-21.

[2] B. Gandham, R. Hill, H.A. Macleod, M. Bowden, Antireflection coatings on solar cells, Sol. Cells. 1 (1979) 3–22.

[3] A. Uzum, M. Kuriyama, H. Kanda, Y. Kimura, Sprayed and spin-coated multilayer antireflection coating films for nonvacuum processed crystalline silicon solar cells, Int. J. Photoenergy. 2 (2017) 1-5.

[4] J.W. Leem, D.H. Jun, J. Heo, W.K. Park, J.H. Park, Single-material zinc sulfide bilayer antireflection coatings for GaAs solar cells, J. Opt. Express 21 (2013) 821–828.

[6] N. Kaiser, Review of the fundamentals of thin-film growth, Appl. Opt. 41 (2002) 3053–3060.

[7] L. Abelmann, C. Lodder, Oblique evaporation and surface diffusion, Thin Solid Films. 305 (1997) 1–21.

[8] R. Swanepoel, Determination of the thickness and optical constants of amorphous silicon, J. Phys. E. 16 (1983) 1214.

[9] M. H. Maleki, H. R. Dizaji, A. Ghorbani, Improving Anti-Reflection MgF_2 Thin Films by Laser Shock Peening and Investigation of its Laser Damage Threshold, J. Appl. Spectrosc. 82 (2015) 58-62.

[10] M. Gholizadeh, R. Zarei Moghadam, A.A. Mohammadi, M.H. Ehsani, H. Rezagholipour Dizaji, Design and fabrication of MgF_2 single-layer antireflection coating by glancing angle deposition, Mater. Res. Innov. 24 (2020) 442-446.

[11] M.H. Ehsani, R.Z. Moghadam, H.R. Dizaji, P. Kameli, Surface modification of ZnS films by applying an external magnetic field in vacuum chamber, Mater Res Express. 4 (2017) 096408.

[12] N. Tajik, M.H. Ehsani, R.Z. Moghadam, H.R. Dizaji, Effect of GLAD technique on optical properties of ZnS multilayer antireflection coatings, Mater Res Bull. 100 (2018) 265-274.

[13] B. Liu, R. Luo, Q. Liang, Y. Zheng, B. Li, J. Zhang, W. Li, L. Wu, L. Feng, Preparation of novel CdS/ZnS composite window layer for CdTe thin film solar cell, J. Mater. Sci. Mater. Electron. 26 (2015) 9985.

[14] X. Wang, H. Huang, B. Liang, Z. Liu, D. Chen, G. Shen, ZnS nanostructures: synthesis, properties, and applications, Crit. Rev. Solid State Mater. Sci. 38 (2013) 57–90.

[15] S. Ummartyotin, Y. Infahsaeng, a comprehensive review on ZnS: from synthesis to an approach on solar cell, Renew. Sust. Energ. Rev. 55 (2016) 17- 24.

[16] D. Hass, Y. Marciano and H. Wadley, Physical vapor deposition on cylindrical substrates, Surf. Coat. Technol. 185 (2004) 283-291.

[17] M. Panjan, Influence of substrate rotation and target arrangement on the periodicity and uniformity of layered coatings, Surf. Coat. Technol. 235 (2013) 32-44.

[18] G. Oh, E. K. Kim, Analysis of ZnS and MgF_2 layered nanostructures grown by glancing angle deposition for optical design, Nanotechnology 31 (2020) 245301.

[19] S. Essig, C. Allebé, T. Remo, J.F. Geisz, M.A. Steiner, K. Horowitz, L. Barraud, J.S. Ward, M. Schnabel, A. Descoeudres, D.L. Young, Raising the one-sun conversion efficiency of III–V/Si solar cells to 32.8%

for two junctions and 35.9% for three junctions, Nature Energy 2 (2017) 1-9.

[20] S.L. Diedenhofen, G. Grzela, E. Haverkamp, G. Bauhuis, J. Schermer, J.G. Rivas, Broadband and omnidirectional anti-reflection layer for III/V multi-junction solar cells, Sol. Energ. Mater. Sol. C. 101 (2012) 308–14.

[21] A.R. Chowdhuri, D.U. Jin, C.G. Takoudis, SiO2/Si (100) interface characterization using infrared spectroscopy: estimation of substoichiometry and strain, Thin Solid Films 457 (2004) 402-405.

[22] W. Zhang, K. Hu, J. Tu, A. Aierken, D. Xu, G. Song, X. Sun, L. Li, K. Chen, D. Zhang, and Y. Zhuang, Broadband graded refractive index $TiO_2/Al_2O_3/MgF_2$ multilayer antireflection coating for high efficiency multi-junction solar cell, Sol Energy 217 (2021) 271-279.

[23] D. H. Hwang, J. H. Ahn, K. N. Hui, K. S. Hui, Y. G. Son, Structural and optical properties of ZnS thin films deposited by RF magnetron sputtering, Nanoscale Res. Lett. 7 (2012) 26–32.

[24] T. Liu, Y. Li, H. Ke, Y. Qian, Sh. Duo, Y. Hong, X. Sun, Chemical bath co–deposited ZnS film prepared from different zinc salts: $ZnSO_4$–$Zn(CH_3COO)_2$, Zn(NO3)2–Zn(CH3COO)2, or ZnSO4–Zn(NO3)2, J. Mater. Sci. Tech. 32 (2015) 207–217.

[25] O. Ozakın, B. Guzeldir, M. Ali Yıldırım, M. Saglam, A. Ates, Influence of film thickness on structural and optical properties of ZnS thin films obtained by SILAR method and analysis of Zn/ZnS/n-GaAs/In sandwich structure, Phys. Stat. Solidi A. 209 (2012) 687–693.

[26] Ş. Korkmaz, S. Elmas, N. Ekem, S. Pat, M. Z. Balbağ Deposition of MgF_2 thin films for antireflection coating by using thermionic vacuum arc (TVA), Opt. Commun. 285 (2012) 2373-2376.

[27] P. O. Offor, B. A. Okorie, F. I. Ezema, V. S. Aigbodion, C. C. DanielMkpume, A.D.Omaha, Synthesis and characterization of nanocrystalline zinc sulphide thin films by chemical spray pyrolysis, J. Alloy. Compd. 650 (2015) 381-385.

[28] P. P. Hankare, P. A. Chate, D. J. Sathe, A. A. Patil, Structure, Surface morphological and opto-electronic properties of zinc sulphide thin films deposited by dip method, Appl. Surf. Sci. 256 (2009) 81-84.

[29] H. M. M. N. Hennayaka, H. S. Lee, Structural and optical properties of ZnS thin film grown by pulsed electrodeposition, Thin Solid Films. 548 (2013) 86-90.

[30] C. Guo, M. Kong, D. Lin, C. Liu, and B. Li, Microstructure-related properties of magnesium fluoride films at 193nm by oblique-angle deposition, Opt. Express. 21 (2013) 960-967.

[31] M.R. Sazideh, M.H. Ehsani, H.R. Dizaji, R.Z. Moghadam, Substrate-induced changes of structural and optical properties of SnS films prepared by glancing angle deposition, Thin Solid Films. 663 (2018) 85-92.

[32] M.R. Sazideh, H.R. Dizaji, M.H. Ehsani, R.Z. Moghadam, Modification of the morphology and optical properties of SnS films using glancing angle deposition technique, Appl. Surf. Sci. 405 (2017) 514-520.

[33] F.C. Akkari, R. Brini, M. Kanzari, B. Rezig, High absorbing $CuInS_2$ thin films growing by oblique angle incidence deposition in presence of thermal gradient, J. Mater. Sci. 40 (2005) 5751–5755.

[34] Y. Zhong, Y.C. Shin, C.M. Kim, B.G. Lee, E.H. Kim, Y.J. Park, K.M.A. Sobahan, C.K. Hwangbo, Y.P. Lee, T.G. Kim, Optical and electrical properties of indium tin oxide thin films with tilted and spiral microstructures prepared by oblique angle deposition, J. Mater. Res. 23 (2008) 2500–2505.

[35] S. Bruynooghe, D. Tonova, M. Sundermann, T. Koch, U. Schulz, Antireflection coatings combining interference multilayers and a nanoporous MgF_2 top layer prepared by glancing angle deposition, Surf. Coat. Technol. 267 (2015) 40-44.

[36] S.Z. Rahchamani, H.R. Dizaji, M.H. Ehsani, Study of structural and optical properties of ZnS zigzag nanostructured thin films, Appl. Surf. Sci. 356 (2015) 1096-1104.

[37] M. H. Ehsani, N. Tajik, M. R. Sazideh, H. Rezagholipour Dizaji, R. Zarei Moghadam. Tuning filtering properties of SnS films deposited on Glass/ITO substrate using glancing angle deposition technique, Mater. Res. Express. 6 (2019) 096415.

[38] J.I. Pankove, Optical Processes in Semicondutors Courier Corporation, New York: Dover publication institute. (2012).

[39] S.S. Hegde, A.G. Kunjomana, M. Prashantha, C. Kumar, K. Ramesh, Photovoltaic structures using thermally evaporated SnS and CdS thin films, Thin Solid Films. 545 (2013) 543-547.

[41] S. Bhaskar, S.B. Majumder, M. Jain, P.S. Dobal, R.S. Katiyar, Studies on the structural, microstructural and optical properties of sol–gel derived lead lanthanum titanate thin films. Mater. Sci. Eng. B. 87 (2001) 178-190.

[42] K. Punitha R. Sivakumar C. Sanjeeviraja V. Ganesan, Influence of post-deposition heat treatment on optical properties derived from UV–vis of cadmium telluride (CdTe) thin films deposited on amorphous substrate, Appl. Surf. Sci. 344 (2015) 89-100.